



Carboxyl-assisted synthesis of Co nanorods with high energy facet on graphene oxide sheets for efficient photocatalytic hydrogen evolution

Bin Tian ^{a,b}, Wenlong Zhen ^a, Haibo Gao ^c, Xuqiang Zhang ^a, Zhen Li ^{a,b}, Gongxuan Lu ^{a,*}

^a State Key Laboratory for Oxo Synthesis and Selective Oxidation, Lanzhou Institute of Chemical Physics, Chinese Academy of Sciences, Lanzhou 730000, PR China

^b University of Chinese Academy of Science, Beijing 100049, PR China

^c State Key Laboratory of Applied Organic Chemistry, College of Chemistry and Chemical Engineering, Lanzhou University, Lanzhou, PR China



ARTICLE INFO

Article history:

Received 16 June 2016

Received in revised form 19 October 2016

Accepted 25 October 2016

Available online 27 October 2016

Keywords:

Co nanorods

Carboxyl-assisted

High surface energy

Low over-potential

Hydrogen evolution

ABSTRACT

In this paper, Co nanorods with extremely high length to diameter and preferred exposed (101) facet were synthesized by carboxyl-assisted over graphite oxide surface. DFT calculation results indicated that (101) facet Co nanorods exhibited higher surface energy of (101) facets (2.61 J/m^2) than that of (100) planes nanorods (2.46 J/m^2). Such Co nanorods showed very low over-potential for proton reduction, about 0.20 V onset overpotential and 400 and 510 mV at current densities of 2 and 5 mA/cm^2 , and worked as high active co-catalyst for photocatalytic hydrogen evolution. Co (101) nanorods loaded catalyst generated $891.3\text{ }\mu\text{mol H}_2$ in 2 h , while Co nanoparticles only gave $451.6\text{ }\mu\text{mol}$ of hydrogen during same time. The apparent quantum efficiency (AQE) of Co nanorods catalyst achieved 17.4% at 520 nm . This work opened a new strategy for design of with rodlike structure cocatalyst with preferred exposed high surface energy facet for photocatalytic hydrogen evolution reaction though the carboxylation of GO.

© 2016 Elsevier B.V. All rights reserved.

1. Introduction

Graphene oxide (GO), a novel 2D nanomaterial prepared from natural graphite, has recently attracted significant attention due to excellent mechanical, electrical, optical and chemical properties, which is widely used in photocatalytic field [1]. In contrast to pristine graphite, graphene oxide sheets are heavily oxygenated, bearing epoxide functional groups and hydroxyl on their basal planes, in addition to carboxyl groups and carbonyl located at the sheet edges [2]. These groups enable graphite oxide to be functionalized through covalent and noncovalent approaches, hence making it a building block for synthesizing versatile functional materials [1]. In addition, its various oxygen-containing functional groups protect graphene oxide sheets from restacking and agglomeration, make it disperse in water and some other solvents readily [3], specifically, these oxygen-containing functional groups, (especially $-\text{COO}$ species) on the surface of GO could serve as nucleation and anchored sites for nanocrystal growth [4]. This provides a facile way to synthesis nanocrystal/nanocarbon hybrids with priority in exposing some planes.

Precious metal such as Pt is an excellent cocatalyst for hydrogen evolution because of its high activity and low overpotential for proton reduction, but high-cost of noble metals precludes their scale-up [5,6]. In particular, Co-based nanohybrids were discovered to evolve hydrogen in the early 1970s [7]. Since then, numerous cobalt-based cocatalysts have been reported as water reduction or oxidation catalysts. It was reported that Co^{2+} injected into TiO_2 lattice caused significant absorption shift to the visible region compared to pure TiO_2 powder [8,9]. It also showed excellent photocatalytic performance for the HER in the present of metallic cobalt nanoparticles@carbonitride nanotubes complexes as cocatalysts [10]. In recent years, CoP and Co-Pi complexes attracted considerable attention due to their stronger noble metallic properties for hydrogen evolution [11,12]. Moreover, Co-based molecular cocatalysts and their derivatives, such as cobalt porphyrin complexes, cobaloximes, cobalt compounds and hexaaminocobalt complexes were also reported as high-active catalysts for HER. These were proposed as potential candidates for replacing noble-metal cocatalysts. However, the design of stable heterogeneous Co cocatalyst for hydrogen generation is still an attractive challenge. The morphology and crystal-facet-exposed of photocatalysts have recently attracted considerable attention because their photoelectric and photocatalytic properties can be further enhanced or optimized by tailoring the surface atomic structures [13–16]. For example, Li et al. demonstrated that the (100) facets of Pt are much more reactive

* Corresponding author.

E-mail address: gxl@lzb.ac.cn (G. Lu).

than the (111) facets on graphene sheet for the hydrogen evolution from water splitting [17–19]. CoP nanobranches with preferred exposure (111) crystal facets exhibited enhanced photocatalytic activity for the hydrogen evolution reaction (HER) compared to other facets [20]. However, as far as we know there is a little report about the effect of Co catalyst with exposure different planes for the activity of hydrogen evolution.

Herein, we synthesized CoNRs/GO nanocomposites with main exposure Co (101) plane by controlling the $-\text{COO}$ species on GO sheets. Meanwhile, we acquired CoNRs with different length to diameter ratio by controlling carboxylation time. Furthermore, DFT calculation results indicated that (101) facet Co nanorods exhibited higher surface energy of (101) facets (2.61 J/m^2) than that of (100) planes (2.46 J/m^2). Such Co nanorods showed very low overpotential for proton reduction, about 0.20 V onset overpotential and 400 and 510 mV at current densities of 2 and 5 mA/cm^2 , and worked as high active co-catalyst for photocatalytic hydrogen evolution. Co (101) nanorods loaded catalyst generated $891.3\text{ }\mu\text{mol H}_2$ in 2 h , while Co nanoparticles only gave $451.6\text{ }\mu\text{mol}$ of hydrogen during same time. The apparent quantum efficiency (AQE) of Co nanorods catalyst achieved 17.4% at 520 nm . This work opened a news strategy for design of with rodlike structure cocatalyst with preferred exposed high surface energy facet for photocatalytic hydrogen evolution reaction though the carboxylation of GO.

2. Experimental section

2.1. Synthesis of carboxylic graphite oxide (GO-OOH)

GO was prepared from natural graphite by a modified Hummers method [21] (detailed see Supporting information). The GO (0.1 g) was dispersed in 250 mL of deionized water and ultrasonic treatment for 1 h up to yellow transparent colloidal solution was regained. Then NaOH (2 g) and ClCH_2COOH (1.5 g) were added, respectively under the condition of stirring, and then the mixture solution was stirred at $50\text{ }^\circ\text{C}$ for 1 h and ultrasonic treatment for $0.5, 2, 3$, and 4 h , respectively. Behind, 10 mL 0.1 M diluted HCl was added into the aforementioned mixture solution and stirred 2 h at room temperature. Followed the solution was washed repeatedly to remove surplus ions until the pH of filtrate become neutral. Vacuum dried was conducted at $60\text{ }^\circ\text{C}$ to harvest GO-OOH.

Synthesis of catalysts and measurements of photocatalytic H_2 evolution activity and apparent quantum efficiency (AQE)

Synthesis of CoNRs/GO-OOH and measurements of the photocatalytic H_2 evolution activity were performed in a sealed Pyrex flask (170 mL) with a flat window (an efficient irradiation area of 10.2 cm^2) and a silicone rubber septum for sampling. Co/GO, Co/RGO and Pt/RGO were used for comparison. 6 mg of GO-OOH was dispersed into 100 mL of TEOA- H_2O solution ($10\%, \text{v/v}$, pH 11) with the ultrasound treatment (25 kHz , 250 W) about 8 min , the calculated amount of aqueous CoSO_4 or solid $\text{H}_2\text{PtCl}_6 \cdot 6\text{H}_2\text{O}$ and Eosin Y (EY) ($1 \times 10^{-3}\text{ mol L}^{-1}$) were added in proper sequence under stirring conditions and each addition followed by magnetic stirring for 30 min . The light source is a 300-W Xenon lamp, which equipped with a 420 nm cutoff filter. Prior to irradiation, the reactant mixture solution was degassed by bubbling Ar gas for 30 min . The amount of hydrogen evolution was measured using gas chromatography (Agilent 6820, TCD, $13 \times$ column, Ar carrier). The AQE was measured under the same photocatalytic reaction conditions with irradiation light through a band-pass filter ($430, 460, 490, 520$, or 550 nm). Photon flux of the incident light was determined using a Ray virtual radiation actinometer (FU 100, silicon ray detector, light spectrum, 400 – 700 nm ; sensitivity, 10 – $50\text{ }\mu\text{V }\mu\text{mol}^{-1}\text{ m}^{-2}\text{ s}^{-1}$). The reaction

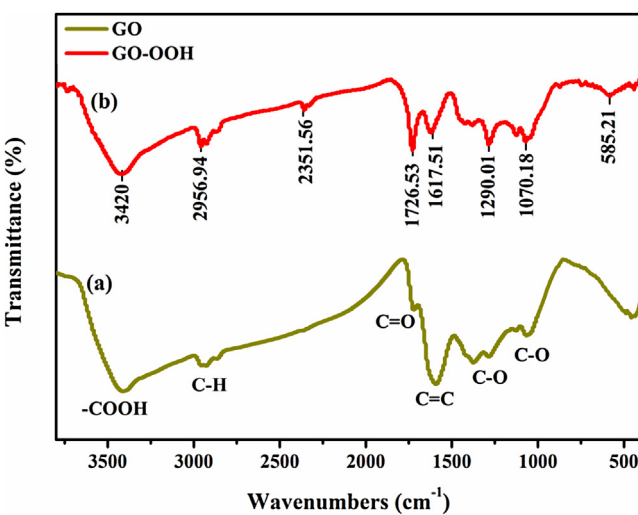


Fig. 1. The FTIR spectrum of (a) GO, (b) GO-OOH.

solutions were irradiated for 0.5 h with bandpass filters for AQE measurements on the H_2 evolution. The following equation was used to calculate the AQE.

$$\text{AQE} = \frac{2 \times \text{the number of evolved hydrogen molecules}}{\text{the number of incident photons}} \times 100\%$$

3. Results and discussion

In order to confirm the variation of oxygen-containing functional groups on the GO after carboxylation treatment, the Fourier transform infrared spectra (FTIR) experiments were executed and analyzed. It could be observed from Fig. 1 curve a that GO exhibited several characteristic absorption bands of oxygen containing groups. The peaks at 1070 cm^{-1} and 1290 cm^{-1} are attributed to $\text{C}=\text{O}$ and $\text{C}=\text{O}-\text{C}$ stretching modes, respectively. The $\text{C}=\text{C}$ skeleton vibration peak could be observed around 1617 cm^{-1} . The IR absorption at about 1726 cm^{-1} could be assigned to the $\text{C}=\text{O}$ stretching vibration and The weak absorption peak at 2351 cm^{-1} was probably from the stretching vibrations of $\text{C}=\text{O}$ double bond to carbon dioxide. The intense peak by $\text{C}-\text{H}$ stretching vibrations was at about 2957 cm^{-1} . The broad peak in the range of 3000 – 3500 cm^{-1} was attributed to the $\text{O}-\text{H}$ stretching vibrations of the $\text{C}-\text{OH}$ groups and the absorption band at low frequency side at 400 – 700 cm^{-1} appeared due to in-plane and out-of-plane bending modes of COO -groups. Similar FTIR pattern was obtained for GO by previous literature [22]. The FTIR spectrum of GO-OOH in Fig. 1 curve b showed a band at about 581 cm^{-1} , which reflects the bending modes of COO -groups, and the peaks relative intensity of oxygen-containing functional groups ($-\text{COOH}$, $\text{C}=\text{O}$ and $\text{C}-\text{O}$) exhibited remarkable enhancement compared to GO. Moreover, it was found that with the increasing of carboxylation time, the peaks relative intensity of oxygen-containing functional groups gradually enhanced (Fig. S1 in the Supplementary material). These results indicated that the oxygen-containing functional groups ($-\text{COOH}$) did increase after carboxylation treatment for GO.

Raman spectrum is considered as an efficient tool for the characterization of carbon nanomaterials particularly graphene, and Fig. 2 showed the Raman spectrum of the GO and GO-OOH. Raman spectrum of GO (Fig. 2 curve a) showed the peaks at 1328 and 1593 cm^{-1} which were typical D and G bands respectively. The G band was the characteristics of all sp^2 carbon forms and provided the information on in plane vibration of the sp^2 carbon atoms [23,24]. The D band indicated the presence of sp^3 defects. The intensity ratio of the D band to G band ($I_G/I_D = 0.783$) showed an indication of disorder in

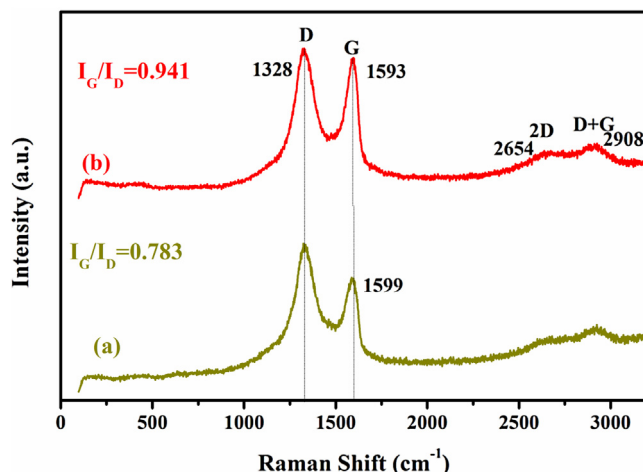
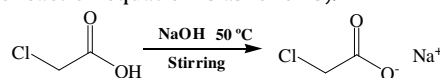


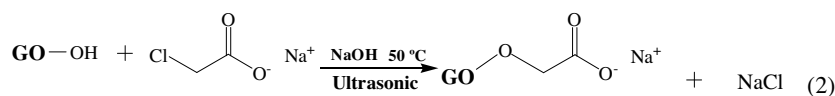
Fig. 2. The Raman spectrum of (a) GO, (b) GO-OOH.

GO carbon materials originating from the defects associated with the vacancies, grain boundaries and amorphous carbon [23]. Apart from that hump like peaks also can be seen at 2654 and 2908 cm⁻¹ which are the second order feature of the D band and G band known as 2D and D + G band. Compared with GO, the I_G/I_D for GO-OOH was found to be ~ 1 (0.941), and the position of G band shifted (about 6 cm⁻¹). These results indicated that the defects on the GO surface decreased might result from modification of carboxyl, and the I_G/I_D increased with the extension of carboxylation time in agreement with the conjecture above (Fig. S2 in the Supplementary material). Furthermore, hump like structure of the 2D-band confirmed the formation of few-layer of GO-OOH [25,26].

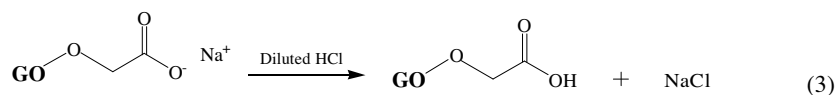
Based on all the results above, we speculated the carboxylation process of graphite oxide mainly undergo the following three processes, firstly, monochloro acetic acid transformed into sodium monochloroacetate under the condition of alkalinity at 50 °C. Then, The chloride ion on sodium monochloroacetate was eliminated under the action of NaOH, and the formation of C⁺ perssadt attacked the –OH on the surface of GO, formed GO–O–sodium acetate compounds (namely S_N1 reaction). Then, the compounds transformed into the ultimate product through the acidification of diluted hydrochloric acid (specific reaction equation is as follows).



(1)



(2)



(3)

The CoNRs/GO-OOH nanohybrids were prepared by in situ photochemical deposition method. The surface morphologies and microstructure of catalysts were characterized *via* transmission electron microscopy (TEM) and high-resolution TEM (HRTEM) as shown in Fig. 3. A typical TEM image of CoNRs/GO-OOH (Fig. 3a) exhibits that a large amount of Co nanorods uniformly deposition the surface of GO-OOH sheets with the length about 30 nm and width ~ 4 nm indicated that CoNRs have a compact contact with RGO sheets. The HRTEM image of CoNRs/GO-OOH shown in Fig. 3b reveals that clearly lattice fringes of CoNRs, suggested that good crystallinity of CoNRs, and the d-spacing of 0.192 nm can be indexed to the (101) planes of hexagonal Co lattice, which

are consistent with the result of X-Ray Diffraction analysis [JCPDS no. 89-4308]. In order to illustrate the influence of functional groups on graphite oxide (GO) surface for the growth of CoNRs, we successfully fabricated CoNRs with different length-diameter ratio through controlled different carboxylation time, suggested that the CoNRs become longer and longer with the extension of carboxylation time (see Fig. S3 in the Supplementary material). In addition, Energy-dispersive X-ray spectroscopy (EDS) recorded from nanohybrid confirmed the presence mainly of Co, C and O elements in the catalysts (Fig. S4 in the Supplementary material). In order to further explain the composition and element distribution of the catalysts, elemental mapping analysis was carried out. As shown in Fig. 3c, the left image shows the TEM of the region where elemental mapping was executed. The red, orange and yellow colors in image correspond to the mapping of cobalt, oxygen and carbon elements, respectively. It was observed that all three elements existed in the catalysts in agreement with the results of EDS, and the distribution of element cobalt in the photocatalyst mainly exist through rod form and an obvious separation could be seen in the distribution of cobalt and oxygen elements, indicated that the active component in photocatalysts mainly exist through metal state cobalt. In addition, the distribution ranges of carbon and oxygen elements were uniformly dispersed in photocatalysts, which could be assigned to the composition of GO.

The formation of Co nanorod-like structure could be attributed to follow an oriented attachment mechanism [27–29]. In this process, the –COOH species have significant roles on the formation of Co nanorods (similar to the role of transfer RNA). As elucidated in Scheme 1, firstly, after carboxylic treatment for GO, it transformed into GO-OOH (Detailed see Experiment Section), then Co²⁺ were adsorbed onto the sites of –COO species through coulomb forces because of surplus negative charge of –COO species, formed cobalt acetate species on the GO-OOH surface [30], which could be confirmed via FTIR spectrum (Fig. S5 in the Supplementary material). These Co ions were reduced to Co metal atoms under the condition of visible light irradiation and photoreductant (EY). Then, GO-OOH sheets would occur self-scrolling on the surface of Co NPs because of nanoparticles induced effect [31], formed a GO-OOH roll subsequently. In addition, Co metal atom would fell off from carboxyl because of loss of positive charges, meanwhile, these –COO species restored the electronegative and would absorb the free Co²⁺ in the

GO-OOH roll. Co²⁺ was reduced to Co atom similarly followed and formed Co–Co metal bond with adjacent cobalt atom, leaded to the formation of CoNRs eventually. Furthermore, CoNRs would be squeezed out from the GO-OOH roll after Co induced double-deck GO-OOH self-scrolling [32]. These speculate were consistent with the results of TEM test, possessed double-deck structure (see Fig. 3a inset). In the formation of CoNRs process, we hold that the smoothing process took place when two faceted, such as (101) plane, came into contact provided the symmetry-breaking necessary for the rod formation. The alternate convex and concave regions that were

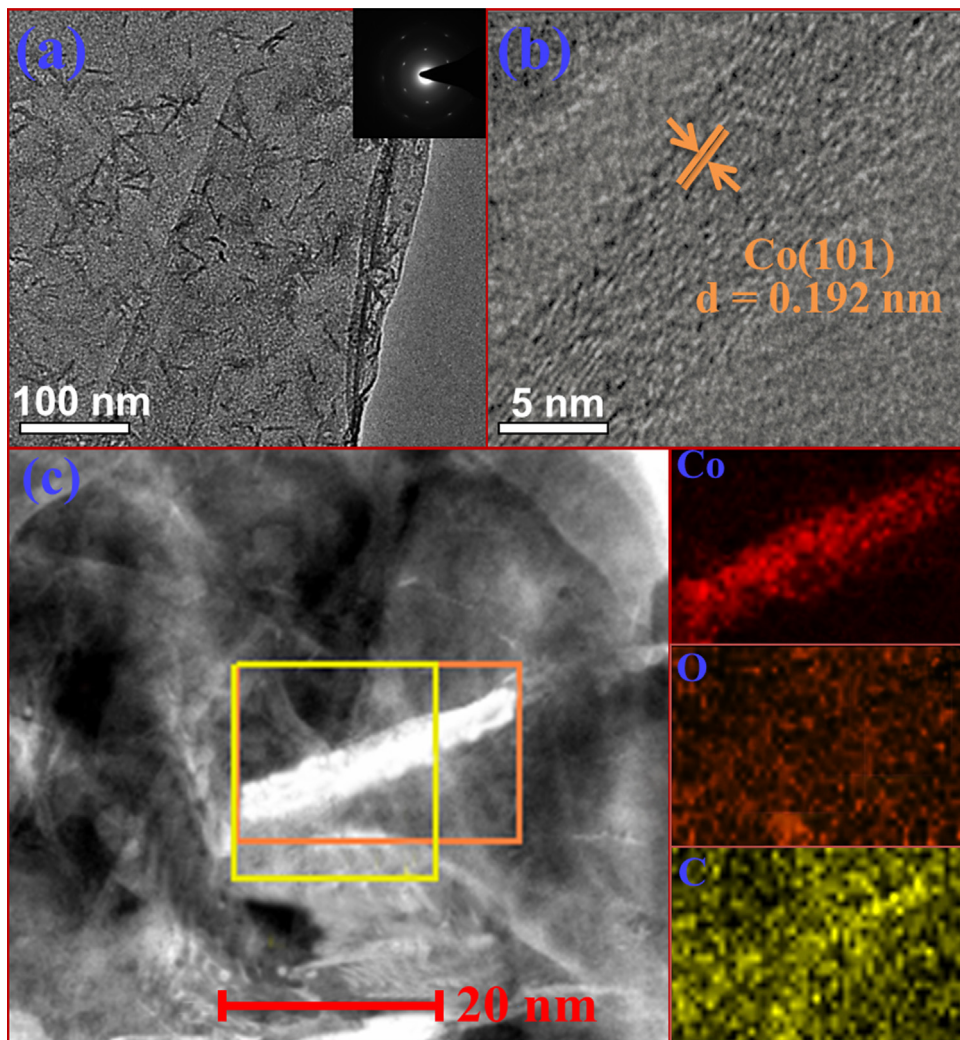
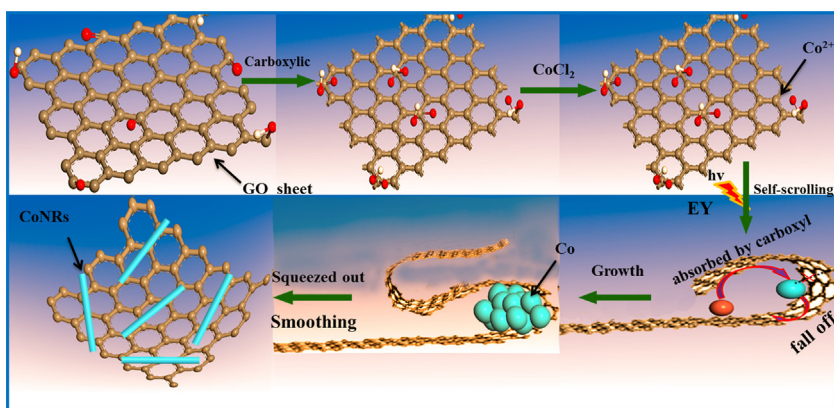


Fig. 3. (a) TEM image for CoNRs/GO-OOH nanohybrid and selected area electron diffraction (SAED) inset. (b) HRTEM image for CoNRs/GO-OOH nanohybrid. (c) Element mapping analysis for CoNRs/GO-OOH catalyst.



Scheme 1. Formation Mechanism of CoNRs/GO-OOH Nanocomposite.

formed lead to a difference in chemical potential which resulted in a smoothing of the particles by diffusion. This process of neck-growth had been investigated extensively both theoretically and experimentally in the context of the sintering of particles [33–35]. In the present case, the smoothing results in the formation of a nearly circular cross section for the growing particle. The length

and width of CoNRs was limited might because of the limit domain effect of graphene [36,37].

To further explain the effect of oxygen-containing functional groups on GO surface for the growth of catalysts, we tested the X-ray diffraction (XRD) pattern. As displayed in Fig. 4, the results of XRD clearly show that all of the diffraction peaks of the hexagonal structure of Co metal (JCPDS no. 89-4308, space group P63/mmc,

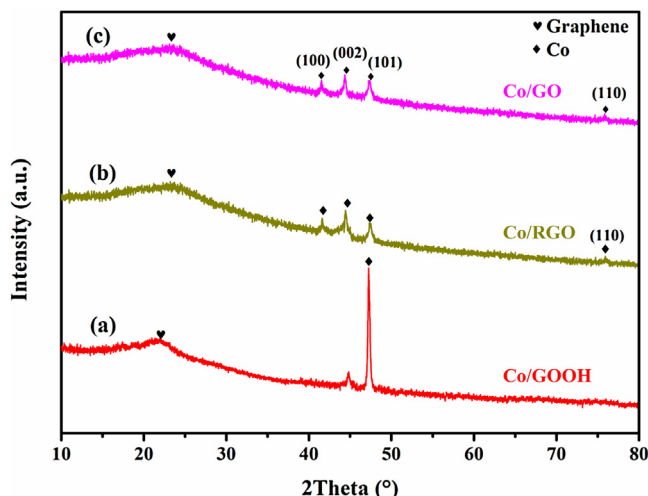


Fig. 4. XRD pattern of (a) CoNRs/GOOH nanohybrid, (b) CoNPs/RGO nanohybrid, (c) CoNPs/GO nanohybrid.

$a = b = 2.505 \text{ \AA}$, $c = 4.089 \text{ \AA}$). However, it is worth noting that obvious changes in the intensity ratios for various peaks were observed, giving further support to the above TEM observations. More specifically, in the case of Co/GO-OOH, the intensity ratio of 6.3 for the (101) and (002) diffractions was remarkably higher than the Co/GO powder intensity ratio (0.57), confirming that the CoNRs are primarily composed of (101) crystalline planes after carboxylation treated, and with the extension of carboxylation time the percentage of (101) planes showed an obviously increasing tendency.

To shed more light on the existence state of CoNRs, we then examined the charged nature of Co in the CoNRs by X-ray photoelectron spectroscopy (XPS) experiments. Fig. 5 shows XPS spectra of the survey window (Fig. 5a), Co 2p window, C 1s window and, O 1s window which corrected by C signal (284.8 eV). Two peaks were apparent in the Co 2p (Fig. 5b) region at 778.5 (2p_{3/2}) and 793.8 (2p_{1/2}) eV. The peaks at 778.5 eV could be assigned to metal state Co (Co⁰), which was positively shifted from that of Co⁰ (777.9), indicated that there are the interaction between CoNRs and GO-OOH result from the so-called coelectron charge interaction, similarly to that of the previous report [38–40]. In addition, the Raman spectrum also confirmed the Co element mainly existed with metallic state in our photocatalysts (Fig. S6 in the Supplementary material). The deconvoluted C 1s signal in Fig. 5c showed a slightly asymmetric tail at higher binding energy, which is a common characteristic for graphite carbon materials [41]. The main peak at 284.8 was assigned to sp²-hybridized graphite-like carbon (C–C sp²), and the peaks centered at 286.4 and 289.3 eV were attributed to surface oxygen groups (designated as C–O–C and –O–C=O, respectively) [42,43]. Furthermore, it was found that the surface oxygen functional groups relative content on photocatalysts gradually increased with increasing carboxylation time from 0.5 to 4 h under the same condition (Fig. S7 and Table S1 in the Supplementary material), indicated that the oxygen-containing functional groups on the graphite carbon materials surface play an important role on the process of crystal growth, in agreement with the results observed on TEM and XRD. The O 1s XPS spectra are shown in Fig. 5d. The CoNRs/GO-OOH nanohybrid had a peak near 530.1 eV, attributed to the lattice O²⁻ in partial oxydic CoNRs on the surface, and the peaks centered at 532.4 and 534.1 eV could be attributed to oxygen-containing functional groups on the GO surface [44–46], consistent with the results of above. Meanwhile, the peak intensity of the oxygen-containing functional groups increased dramatically compared with previous studies, indicating that many more

oxygen-containing functional groups were created on the GO surface through the carboxyl treated [21].

The photocatalytic behaviors of the CoNRs/GO-OOH catalyst was carried out by measure the amount of H₂ evolution under visible light irradiation. For comparison, the performances of Co/RGO and Co/GO were also investigated. As shown in Fig. 6a, it can be clearly seen that unlike the Co/RGO catalyst, CoNRs/GO-OOH and Co/GO photocatalysts exhibited excellent photocatalytic activities for the hydrogen evolution reaction (HER). Among them, the CoNRs exhibited the highest photocatalytic activity, as it could generate 891.3 μmol H₂ in 2 h, which reached the same number as Pt/RGO under visible-light irradiation [21]. In contrast, Co/GO produced 556.4 μmol H₂ in 2 h, indicated that the (101) planes of CoNRs showed the higher hydrogen generation activity than other planes in agreement with characterization of the above. We also studied the influence of CoNRs weight ratio to GO-OOH on hydrogen evolution activity. The highest photocatalysis activity was reached when the ratio was 1/2 (Fig. 6b). Further increase of that ratio resulted in a slight decreased, which might result from the decrease of the GO-OOH absorption site to EY in the photocatalysis system.

The effect of pH on photocatalytic activity of CoNRs/GO-OOH for hydrogen generation was also researched, indicated that the CoNRs/GO-OOH nanohybrid was insensitive to pH the rang from 8 to 12, and the hydrogen evolution activity was the highest at pH 11 (Fig. S8 in the Supplementary material). The amount of hydrogen was decrease when the solution was held under the strong acid or alkaline condition (pH 3 and 13). The possible reason was that the protonation of TEOA, which was rendered an inefficient electron donor, led to a short lifetime for EY³⁺ in more acidic solutions. Then resulted in the concentration of reductively quench EY³⁺ become low, which was not conducive to the evolution of hydrogen from water. In addition, the carboxyl groups of EY might appeared deprotonate under the condition of strongly basic and the dye could not be adsorbed on GO-OOH effectively because of electrostatic repulsion resulted in a relatively low hydrogen evolution activity [47].

The stability of the Co/GO-OOH nanohybrids was evaluated, and the results were shown in Fig. 6c. Our results showed that CoNRs/GO-OOH nanohybrid exhibited a higher stability than Pt/RGO (Fig. S9 in the Supplementary material), and could maintain its activity at least 8 h. In addition, as shown in Fig. 6d, the highest apparent quantum efficiencies (AQE) reached 17.4% at 520 nm for CoNRs/GO-OOH system, which corresponded to the strongest absorption wavelength of EY at 515 nm (Fig. S10 in the Supplementary material). However, the second high AQE was appeared at 430 nm might ascribe to its stronger photon energy [21].

In order to clarify the underlying mechanism for the higher photocatalytic activity of CoNRs relative to CoNPs, we studied the surface structures and surface energies of Co (101) and other planes through density functional theory (DFT) calculations (detailed see Support information and Table S2). Our surface models for both the (101) and (100) surfaces were constructed on the basis of a slab model including 40 atoms of Co (101) with a vacuum region having the same thickness as Co (100). Furthermore, each surface was cut to create a nonpolar surface, with atomic stoichiometry satisfied within the each side of the slab. Geometry relaxations were performed with the midlayers fixed. The surface energy (γ) was computed using the formula as follow.

$$\gamma = \frac{E_{\text{slab}} - nE_{\text{bulk}}}{2A}$$

where E_{slab} is the total energy of the slab, E_{bulk} is the total energy of the bulk per unit cell, n is the number of bulk unit cells contained in the slab, and A is the surface area of each side of the slab. The calculation results showed that the surface energy of (101) facets (2.61 J/m²) is higher than that of (100) facets (2.46 J/m²),

indicating that the (101) facets should be more reactive than (100) facets, which is consistent with the results of activity measurement (Table S3 in the Supplementary material). On the basis of the above calculations, we speculated that each CoNRs possesses highly reactive (101) facets and a high density of corners, edges, and defects, which may markedly increase charge transport and the number of catalytically active sites on their surfaces, and then facilitate the adsorption of $\text{H}_2\text{O}/\text{H}^+$ on these sites. Thereby, the hydrogen evolution reaction between the adsorbed H and photogenerated electrons could proceed more rapidly under visible light irradiation, which may result in a higher photocatalytic activity for HER.

In order to confirm CoNRs (101) planes played a significant role on charge transport, photoluminescence and time-resolved photoluminescence (TRPL) were executed. Fig. 7a exhibits a distinct emission peak at about 530 nm in EY- H_2O solution, which is consistent with previous reports [48]. These emissions were dramatically quenching as the introduction of catalysts, and the quenching efficiency of CoNRs/GO-OOH (66.0%) was remarkably higher than other due to the rapid transfer of photogenerated electrons from EY to graphene and CoNRs, and then improved the photocatalytic activity subsequently. Meanwhile, slight bathochromic-shift were observed in EY/Co/GO and EY/Co/GO-OOH system, which could be attribute to the noncovalent interaction of GO-OOH and CoNRs with EY [21]. The Fig. 7b further showed the lifetime of EY/Co/GO and EY/Co/GO-OOH were longer than that of EY, and EY/Co/GO-OOH system possessed the longest lifetime, indicated that the CoNRs (101) facet was advantageous to capture photo-induced electronic, thus achieved the goal of charge separation and the data of fluorescence lifetimes see Table S4 in the Supplementary material, in agreement with results above.

To further illustrate the effect of CoNRs (101) acceleration charges transport, electrochemical experiments were carried out, included Linear sweep voltammetry (LSV), Transient photocurrent-time and electrochemical impedance spectroscopy (EIS). For comparison, Co/RGO and Co/GO were also tested. The LSVs plot recorded with CoNRs/GO-OOH nanohybrid on ITO glassy electrodes showed the smaller onset overpotential ($\sim 0.20\text{ V}$) than Co/GO (~ 0.34) and Co/RGO (~ 0.40) for the HER (Fig. 8a), beyond which the cathodic current rose rapidly under more negative potentials and only required overpotentials of 400 and 700 mV to reach current densities of 2 and $10\text{ mA}/\text{cm}^2$, respectively. Fig. 8b showed dramatically enhancement in photocurrent with CoNRs/GO-OOH in relative to Co/RGO and Co/GO, indicated that the electrons transfer from EY $^{\bullet-}$ to CoNRs/GO-OOH was fast as well as that to the ITO glass, and as excellent electrons acceptor and transporter, CoNRs/GO-OOH nanohybrid efficiently extended the lifetime of photo-generated electrons, and thus the hydrogen generation activity was improved. All these result indicated that the introduction of CoNRs (101) promoted the electrons transfer from the supporter in agreement with the CoNRs/GO-OOH system possessed the smallest semicircle in the middle-frequency region compared with those of Co/GO and Co/RGO electrodes under the same condition (Fig. S11 in the Supplementary material). In addition, stability of the catalytic response was also evaluated by cycling the Co/GO-OOH-modified SCE continuously for 1000 cycles. At the end of the cycling procedure, the catalyst affords similar LSV curves to the initial cycle with negligible loss of the cathodic current (Fig. S12 in the Supplementary material).

The mechanism of CoNRs/GO-OOH/EY used for photocatalytic hydrogen evolution was present in Scheme 2. Firstly, EY was com-

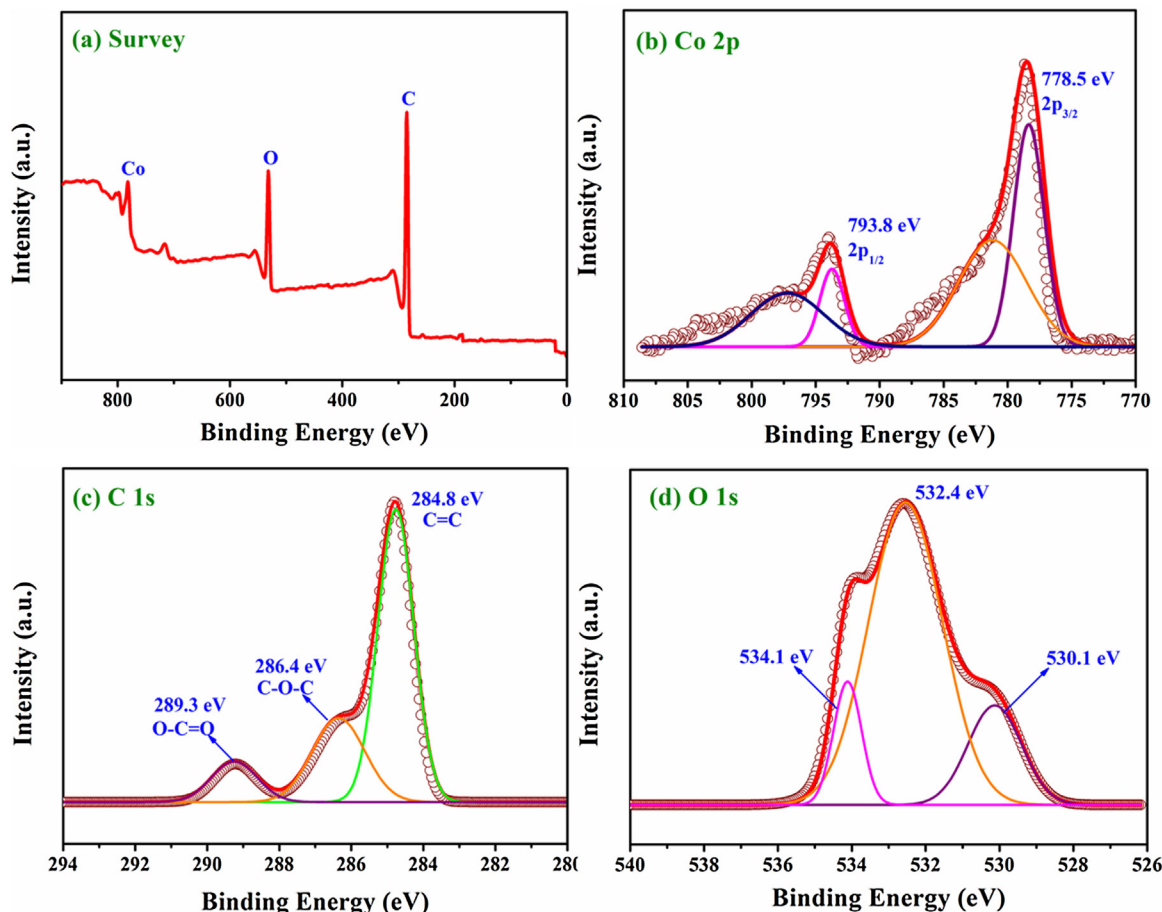


Fig. 5. The XPS spectra of CoNRs/GO-OOH (a) Co 2p, (b) C 1s, (c) O 1s and (d) survey.

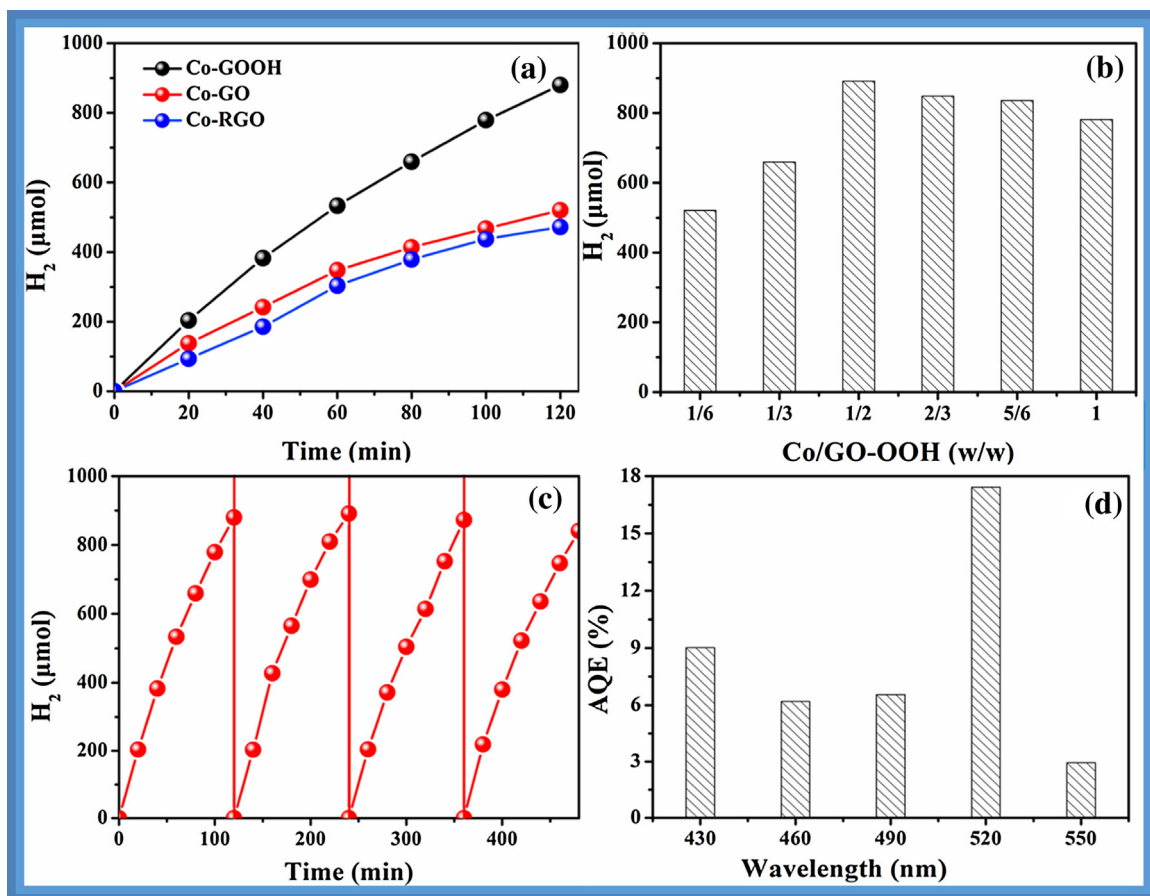


Fig. 6. (a) The amount of hydrogen evolution by EY photosensitized systems catalyzed loaded on the different carrier. (b) The photocatalytic activity of CoNRs/GO-OOH with different weight ratio of CoNRs to GO-OOH (6 mg) for the hydrogen evolution photosensitized by EY, CoNRs/GO-OOH = 1/6, 1/3, 1/2, 2/3, 5/6 and 1, respectively. (c) Stability testing of CoNRs/GO-OOH nanohybrid. (d) Apparent quantum efficiency (AQE) of CoNRs/GO-OOH dye sensitized system under different wavelengths of visible light irradiation (from 430 to 550 nm).

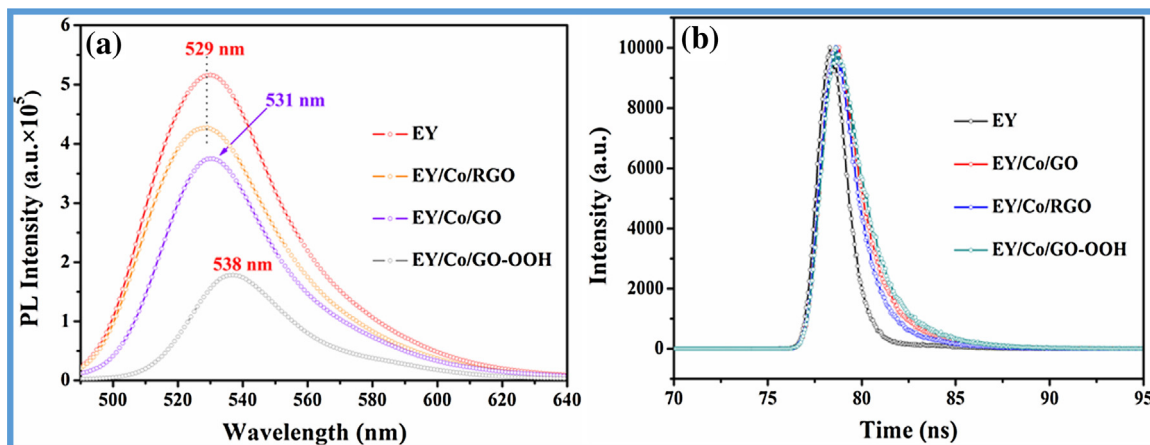


Fig. 7. (a) Photoluminescence and (b) time-resolved photoluminescence (TRPL) spectra of EY, EY/Co/RGO, EY/Co/GO and EY/CoNRs/GO-OOH at an excitation wavelength of 464 nm.

bined with the GO-OOH by the noncovalent π - π interactions under the condition of intense agitation [40]. Then, the excited electrons were input to GO-OOH, transferred to CoNRs very efficiently with the aids of its excellent conductive, and the protons were reduced to hydrogen on CoNRs loaded on the RGO surface. Meanwhile, the adsorbed EY transformed into singlet excited state (EY^{1*}), and subsequently formed a lowest-lying triplet excited state species

(EY^{3*}) by an efficient intersystem crossing (ISC) [21]. The oxidation EY^{3*} could be reductively quenched by sacrificial donor TEOA to EY^{1*} . The electron transfers to the surface of CoNRs, and catalyzed proton reduction to H_2 . Here, high surface energy CoNRs (101) species accelerated photo-production electrons efficient separation, resulted in a high hydrogen evolution activity compared with other facets.

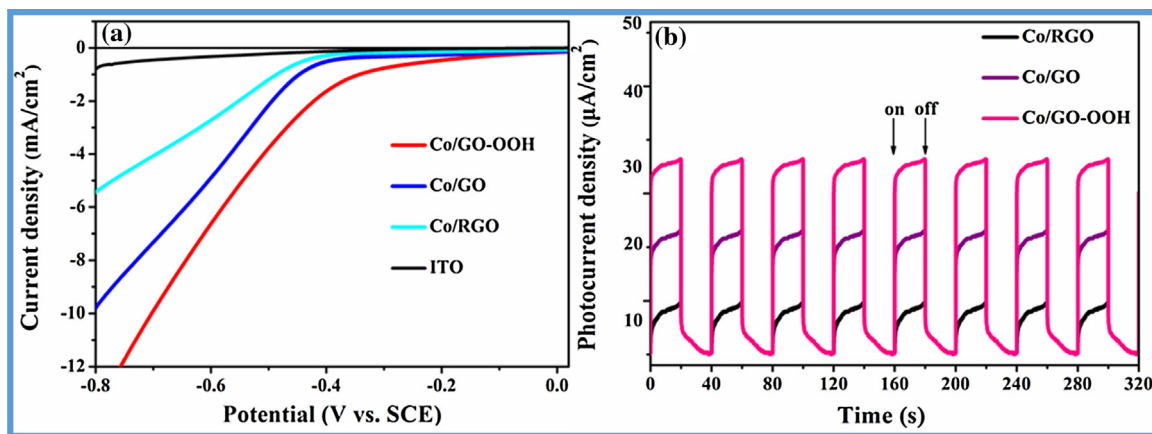
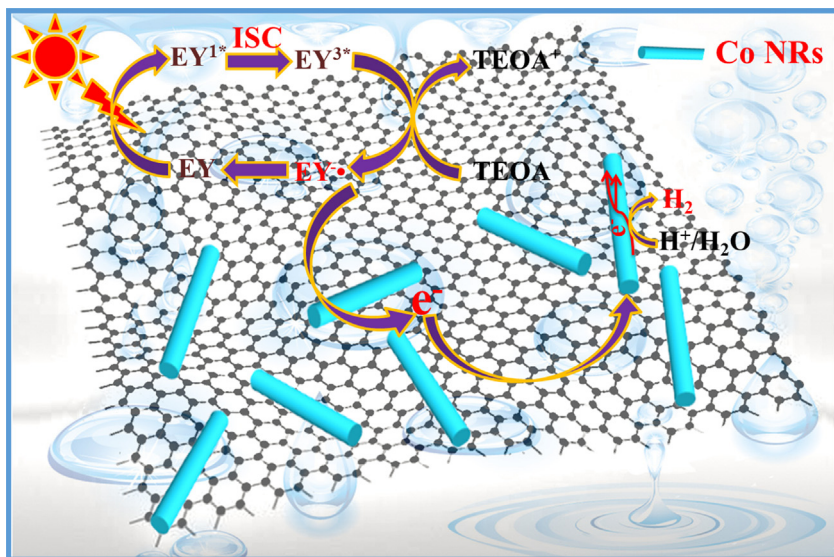


Fig. 8. (a) Linear sweep voltammetry (LSV) curves of bare ITO glass and catalysts coated ITO electrodes and (b) Transient photocurrent-time profile of EY photo-sensitized Co/GO-OOH, Co/GO and Co/RGO coated on ITO glass.



Scheme 2. The Hydrogen Evolution Mechanism of CoNRs/GO-OOH/EY System.

4. Conclusions

In summary, we have demonstrated a facile and efficient process for the shape-selective synthesis of Co photocatalyst that preferential exposure of photocatalytically hydrogen evolution active facets, with rodlike structure and without using any capping agent by the carboxylation of GO. Moreover, DFT calculation results indicated that (101) facet Co nanorods exhibited higher surface energy of (101) facets (2.61 J/m²) than that of (100) planes nanorods (2.46 J/m²). Such Co nanorods showed very low overpotential for proton reduction, about 0.20 V onset overpotential and 400 and 510 mV at current densities of 2 and 5 mA/cm², and worked as high active co-catalyst for photocatalytic hydrogen evolution. Co (101) nanorods loaded catalyst generated 891.3 μmol H₂ in 2 h, while Co nanoparticles only gave 451.6 μmol of hydrogen during same time. The apparent quantum efficiency (AQE) of Co nanorods catalyst achieved 17.4% at 520 nm. This work opened a new strategy for design of with rodlike structure cocatalyst with preferred exposed high surface energy facet for photocatalytic hydrogen evolution reaction though the carboxylation of GO.

Conflict of interest

The authors declare no competing financial interest.

Acknowledgments

This work has been supported by the National Natural Science Foundation of China (Grant Nos. 21433007 and 21673262) and the 973 Program of Department of Sciences and Technology China (Grant No. 2013CB632404).

Appendix A. Supplementary data

Supplementary data associated with this article can be found, in the online version, at <http://dx.doi.org/10.1016/j.apcatb.2016.10.070>.

References

[1] H. Bao, Y. Pan, Y. Ping, N.G. Sahoo, T. Wu, L. Li, J. Li, L.H. Gan, *Small* 7 (2011) 1569–1578.

[2] S. Stankovich, D.A. Dikin, G.H.B. Dommett, K.M. Kohlhaas, E.J. Zimney, E.A. Stach, R.D. Piner, S.T. Nguyen, R.S. Ruoff, *Nature* 442 (2006) 282–286.

[3] A. Erdem, M. Muti, P. Papakonstantinou, E. Canavar, H. Karadeniz, G. Congur, S. Sharma, *Analyst* 137 (2012) 2129–2135.

[4] Y. Liang, H. Wang, D. Peng, W. Chang, G. Hong, Y. Li, M. Gong, L. Xie, J. Zhou, J. Wang, T.Z. Regier, F. Wei, H. Dai, *J. Am. Chem. Soc.* 134 (2012) 15849–15857.

[5] M.G. Walter, E.L. Warren, J.R. McKone, S.W. Boettcher, Q. Mi, E.A. Santori, N. Lewis, *Chem. Rev.* 110 (2010) 6446–6473.

[6] L. Ma, X. Kang, S. Hu, F. Wang, *J. Mol. Catal. (China)* 29 (2015) 359–368.

[7] P.W. Du, R. Eisenberg, *Energy Environ. Sci.* 5 (2012) 6012–6021.

[8] D. Dvoranová, V. Brezová, M. Mazúra, M.A. Malati, *Appl. Catal. B: Environ.* 37 (2002) 91–105.

[9] C. Li, Z. Lei, Q. Wang, F. Cao, F. Wang, W. Shangguan, *J. Mol. Catal. (China)* 29 (2015) 382–389.

[10] X. Dai, Z. Li, Y. Ma, *ACS Appl. Mater. Interfaces* 8 (2016) 6439–6448.

[11] J. Tian, Q. Liu, A.M. Asiri, X. Sun, *J. Am. Chem. Soc.* 136 (2014) 7587–7590.

[12] M.W. Kanan, D.G. Nocera, *Science* 321 (2008) 1072–1075.

[13] H. Yang, C. Sun, S. Qiao, J. Zou, G. Liu, S. Smith, H. Cheng, G. Lu, *Nature* 453 (2008) 638–641.

[14] G. Liu, C. Sun, H. Yang, S. Smith, L. Wang, G. Lu, H. Cheng, *Chem. Commun.* 46 (2010) 755–757.

[15] G. Liu, H. Yang, X. Wang, L. Cheng, J. Pan, G. Lu, H. Cheng, *J. Am. Chem. Soc.* 131 (2009) 12868–12869.

[16] M. Luo, W. Yao, C. Huang, Q. Wu, Q. Xu, *RSC Adv.* 5 (2015) 40892–40898.

[17] Z. Li, Q. Wang, C. Kong, Y. Wu, Y. Li, G. Lu, *J. Phys. Chem. C* 119 (2015) 13561–13568.

[18] M. Luo, P. Lu, W. Yao, C. Huang, Q. Xu, Q. Wu, Y. Kuwahara, H. Yamashita, *ACS Appl. Mater. Interfaces* 8 (2016) 20667–20674.

[19] M. Luo, W. Yao, C. Huang, Q. Wu, Q. Xu, *J. Mater. Chem. A* 3 (2015) 13884–13891.

[20] E.J. Popczun, C.W. Roske, C.G. Read, J.C. Crompton, J.M. McEnaney, J.F. Callejas, N.S. Lewis, R.E. Schaak, *J. Mater. Chem. A* 3 (2015) 5420–5425.

[21] B. Tian, Z. Li, W. Zhen, G. Lu, *J. Phys. Chem. C* 120 (2016) 6409–6415.

[22] S. Park, D.A. Dikin, S.T. Nguyen, R.S. Ruoff, *J. Phys. Chem. C* 113 (2009) 15801–15804.

[23] W. Zhang, J. Cui, C. Tao, Y. Wu, Z. Li, L. Ma, Y. Wen, G. Li, *Angew. Chem. Int. Ed.* 121 (2009) 5978–5982.

[24] J. Lu, J. Yang, J. Wang, A. Lim, S. Wang, K.P. Loh, *ACS Nano* 3 (2009) 2367–2375.

[25] Y. Zhou, Q. Bao, L. Tang, Y. Zhong, K.P. Loh, *Chem. Mater.* 21 (2009) 2950–2956.

[26] G. Srinivas, Y. Zhu, R. Piner, N. Skipper, M. Ellerby, R. Ruoff, *Carbon* 48 (2010) 630–635.

[27] B. Liu, H. Zeng, *J. Am. Chem. Soc.* 125 (2003) 4430–4431.

[28] N. Pradhan, H.F. Xu, X.G. Peng, *Nano Lett.* 6 (2006) 720–724.

[29] K.S. Cho, D.V. Talapin, W. Gaschler, C.B. Murray, *J. Am. Chem. Soc.* 127 (2005) 7140–7147.

[30] Y. Liang, Y. Li, H. Wang, H. Dai, *J. Am. Chem. Soc.* 135 (2013) 2013–2036.

[31] Y. Li, H. Yu, H. Li, C. An, K. Zhang, K.M. Liew, X. Liu, *J. Phys. Chem. C* 115 (2011) 6229–6234.

[32] W. Li, X. Zheng, B. Liu, X. Sun, T. Wang, J. Zhang, Y. Yan, *Carbon* 89 (2015) 272–278.

[33] V.N. Koparde, P.T. Cummings, *J. Phys. Chem. B* 109 (2005) 24280–24287.

[34] P. Zeng, S. Zajac, P.C. Clapp, J.A. Rifkin, *Mater. Sci. Eng. A* 252 (1998) 301–306.

[35] A. Halder, N. Ravishankar, *Adv. Mater.* 19 (2007) 1854–1858.

[36] O.V. Yazyev, M.I. Katsnelson, *Phys. Rev. Lett.* 100 (2008) 0472091.

[37] W. Yang, G. Chen, Z. Shi, C. Liu, L. Zhang, G. Xie, M. Cheng, D. Wang, R. Yang, D. Shi, K.J. Watanabe, T. Taniguchi, Y. Yao, Y. Zhang, G. Zhang, *Nat. Mater.* 12 (2013) 792–797.

[38] A.B. Mandale, S. Badrinarayanan, S.K. Date, A.P.B. Sinha, *Relat. Phenom.* 33 (1984) 61–72.

[39] X. Yan, L. Tian, M. He, X. Chen, *Nano Lett.* 15 (2015) 6015–6021.

[40] C. Kong, S. Min, G. Lu, *ACS Catal.* 4 (2014) 2763–2769.

[41] X. Zou, L. Zhang, Z. Wang, Y. Luo, *J. Am. Chem. Soc.* 138 (2016) 2064–2077.

[42] L. Zhang, Z. Su, F. Jiang, L. Yang, J. Qian, Y. Zhou, W. Li, M. Hong, *Nanoscale* 6 (2014) 6590–6602.

[43] P. Chen, T. Xiao, Y. Qian, S. Li, S. Yu, *Adv. Mater.* 25 (2013) 3192–3196.

[44] C.D. Wagner, D.A. Zatko, R.H. Raymond, *Anal. Chem.* 52 (1980) 1445–1451.

[45] X. Chen, L. Liu, P. Yu, S. Mao, *Science* 331 (2011) 746–750.

[46] T. Xia, C. Zhang, N.A. Oyler, X. Chen, *Adv. Mater.* 25 (2013) 6905–6910.

[47] W. Zhen, J. Ma, G. Lu, *Appl. Catal. B: Environ.* 190 (2016) 12–25.

[48] W. Zhen, B. Li, G. Lu, J.T. Ma, *Chem. Commun.* 51 (2015) 1728–1731.